ENVIRONMENTAL RESEARCH
LETTERS

LETTER • OPEN ACCESS

Multi-year variation of near-surface ozone at Zhongshan Station, Antarctica

To cite this article: Biao Tian *et al* 2022 *Environ. Res. Lett.* **17** 044003

ENVIRONMENTAL RESEARCH
LETTERS

OPEN ACCESS

RECEIVED
31 December 2021

ACCEPTED FOR PUBLICATION
24 February 2022

PUBLISHED
9 March 2022

LETTER

Multi-year variation of near-surface ozone at Zhongshan Station, Antarctica

Biao Tian[1], Minghu Ding[1,*], Davide Putero[2], Chuanjin Li[3], Dongqi Zhang[1], Jie Tang[1], Xiangdong Zheng[1], Lingen Bian[1] and Cunde Xiao[4]

[1] State Key Laboratory on Severe Weather, Chinese Academy of Meteorological Sciences, Beijing 100081, People's Republic of China
[2] CNR–ISAC, National Research Council of Italy, Institute of Atmospheric Sciences and Climate, corso Fiume 4, 10133 Turin, Italy
[3] State Key Laboratory of Cryospheric Science, Northwest Institute of Eco-Environment and Resources, Chinese Academy of Sciences, Lanzhou 730000, People's Republic of China
[4] State Key Laboratory of Earth Surface Processes and Resource Ecology, Beijing Normal University, Beijing 100875, People's Republic of China
[*] Author to whom any correspondence should be addressed.

E-mail: dingminghu@foxmail.com

Keywords: near-surface ozone (O_3), Zhongshan Station, O_3 enhancement events (OEEs)

Supplementary material for this article is available online

Abstract

With the support of the Chinese National Antarctic Research Expedition, near-surface ozone (O_3) was continuously monitored at Zhongshan Station (ZOS) (69°22′12″ S, 76°21′49″ E, 18.5 m above sea level) in East Antarctica from 2008 to 2020. The seasonal and diurnal variability of near-surface O_3 at ZOS were investigated. O_3 enhancement events (OEEs) were frequently observed in the warm season (OEEs in January accounted for 23.0% of all OEEs). The OEEs at ZOS were related to the photochemical reaction processes under the influences of O_3 and solar radiation in the stratosphere and synoptic-scale air mass transport from coastal areas (Princess Elizabeth Land, Wilkes Land, and Queen Mary Land), as evidenced by the recorded wind speed, solar shortwave irradiance, and total column ozone data and the computed potential source contribution function and concentration-weighted trajectory models. The results computed by the tool Stratosphere-to-Troposphere Exchange Flux indicated that stratosphere-to-troposphere transport had no direct impact on OEEs at ZOS. Therefore, synoptic-scale air mass transport is the main cause of OEEs in Antarctica, which is consistent with previous studies. Unlike OEEs at inland Antarctic stations, which are mainly affected by air mass transport from inland plateaus, OEEs at ZOS, a coastal station, are mainly affected by air mass transport from coastal land in East Antarctica.

1. Introduction

Tropospheric ozone (O_3) is an important short-lived greenhouse gas and a driver of atmospheric oxidation capacity (Schultz *et al* 2015). Within the influence of strong solar radiation ($\lambda < 424$ nm), volatile organic compounds and NO_X ($NO + NO_2$), O_3 is produced photochemically and can accumulate to a hazardous level under favorable meteorological conditions (Wakamatsu *et al* 1996). In the case of NO_X-rich air, NO_2 is accumulated because of reactions between NO and HO_2 or RO_2 (peroxy radicals), and then O_3 accumulates. While in the case of NO_X-poor air, these peroxy radicals react with O_3, leading to loss (Lin *et al* 1988). Because of its high reactivity and short atmospheric residence time, the surface O_3 long-term trend is hard to evaluate (Cooper *et al* 2014, Monks *et al* 2015, Schultz *et al* 2015). This is especially true in Antarctica, a remote region from the human activities. Previous investigations suggested that O_3 production in the Antarctica planetary boundary layer (PBL) is affected by some global and regional climate-related variables, i.e. changes in UV fluxes due to total O_3 variability over Antarctica (e.g. Jones and Wolff 2003, Frey *et al* 2015), variability in long-range air mass transport patterns (e.g. Legrand *et al* 2016), and the

depth of the continental mixing layers. Sometimes, summer episodes of 'O_3 enhancement events' (OEEs) could be observed in the Antarctica interior (e.g. Crawford *et al* 2001, Legrand *et al* 2009, Cristofanelli *et al* 2018) as well as at coastal sites influenced by air mass transport from the interior of the continent (e.g. Cristofanelli *et al* 2011). This phenomenon was attributed to the photodenitrification of the summer snowpack, which can result in NO_X emissions (Davis *et al* 2001) to the atmosphere and subsequent photochemical O_3 production (e.g. $NO_2 + hv \rightarrow NO + O$; $O + O_2 + M \rightarrow O_3 + M$; Jones *et al* 2000, Jones and Wolff 2003, David and Nair 2011). These processes are capable of driving the seasonality of near-surface O_3 over the Antarctic Plateau (e.g. Crawford *et al* 2001, Legrand *et al* 2009), thus potentially providing a significant input of O_3 to the whole Antarctic region (e.g. Legrand *et al* 2016). Indeed, as shown in Cristofanelli *et al* (2008) and Legrand *et al* (2016), due to air mass transport, photochemically produced O_3 in the PBL over the Antarctic Plateau can affect the O_3 variability thousands of km from the emission area.

Moreover, middle and low latitude near-surface O_3 concentrations at high-elevation sites can also be increased by the downward transport of O_3-rich air from upper troposphere and lower stratosphere (e.g. Bonasoni *et al* 2000, Stohl and Sodemann 2010, Yin *et al* 2017). The earliest study, carried out by aircraft flight NSFC-130 over the Ellsworth Mountains of Antarctica in 1978, found that mountainous terrain can induce atmospheric waves that propagate across the tropopause. The tropospheric and stratospheric air may mix, leading to an increase in tropospheric O_3 (e.g. Robinson *et al* 1983). O_3 sounding at the Resolute and Amundsen-Scott Stations (South Pole, SOP) also found the transportation from the stratosphere to the troposphere, the flux of which could reach 5×10^{10} mol cm^{-2} s^{-1} (e.g. Gruzdev and Sitnov 1993). Recently, Traversi *et al* (2017) suggested that the variability of air mass transport from the stratosphere to the Antarctic Plateau can affect nitrate content in the low troposphere and the snowpack, leading to O_3 variation.

In summary, the near-surface O_3 could be affected by many processes, especially the *in-situ* production, synoptic-scale air mass transport, 'deep' Stratosphere-to-Troposphere Transport (STT) events. In 2008, as part of International Polay Year project, Chinese National Antarctic Research Expedition established an on line observation system of atmospheric composition at Zhongshan Station (ZOS), the edge of Lambert glacier basin, east Antarctica (figure 1). Based on the data, only general characteristics of near-surface O_3 have been introduced (e.g. Wang *et al* 2011, Bian *et al* 2018). Thus in this paper, the detailed source and sink mechanism was analyzed combined with meteorology, solar shortwave irradiance, and total column O_3 (TCO) experiments.

2. Description of sites and methods

2.1. Sites and instruments

The online observation system of atmospheric composition were installed at the Swan Ridge (69°22′12″ S, 76°21′49″ E, 18.5 m a.s.l.), northwest of the Nella fjord. Strong E or ENE winds (45°–135°) dominate here, occupying 92% of time (Wang *et al* 2011). It implies human pollution from ZOS is weak.

In January 2008, an EC9810A ultraviolet photometric absorption O_3 analyzer was deployed to monitoring near-surface O_3, with an EC9811 as calibrator. Unfortunately, the instrument encountered a failure in January 2014, and the data was not credible till January 2016 when a TE49i ultraviolet photometric absorption O_3 analyzer and a TE49ips ultraviolet photometric absorption O_3 calibrator (Thermo Company) replaced. The measurement frequency was 1 min. Data are available at https://doi.org/10.11856/SNS.D.2021.001.v0. The meteorological monitoring including solar shortwave irradiance, wind speed was started in 1989 according to the World Meteorological Organization requirements. The Brewer monitoring including TCO was started in 1993 according to the World Ozone and Ultraviolet Radiation Data Centre.

2.2. Calibration process and results

In general, the zero-point, range and operating parameters of the O_3 analyzer should be checked regularly and before each operation. The calibration procedure followed the China's environmental protection standard 'ambient air—determination of O_3—ultraviolet method' (HJ590-2010) (www.mee.gov.cn/gkml/sthjbgw/sthjbgg/201808/t20180815_451411.htm), which is stricter than the standards of the U.S. Environmental Protection Agency (www.epa.gov/ttn/amtic/files/ambient/pm25/qa/ QAHandbook-Vol-II.pdf.): the slope of the calibration curve ranged between 0.95 and 1.05, and the intercept ranged between −5 and 5 ppb. Every 3 months in ZOS, five standard concentrations of O_3 gas were generated for each calibration. From 2008 to 2020, 44 calibrations were made (e.g. excluding 2014 and 2015 data due to instrumental failure and it can be seen in supplement 1 available online at stacks.iop.org/ERL/17/044003/mmedia for the detailed results), and the correlation coefficient r was greater than 0.999 for the calibration quality of the observed data.

Furthermore, a variance test was applied to remove abnormal data based on the Laida criterion method, which assumes that the records obey a normal distribution. The formula is $|xi - x| > 3\sigma$, where xi is the measured value, x is the time series mean and σ is the standard deviation. After processing, 99.2% of the hourly mean data were retained from ZOS time series (excluding 2014 and 2015).

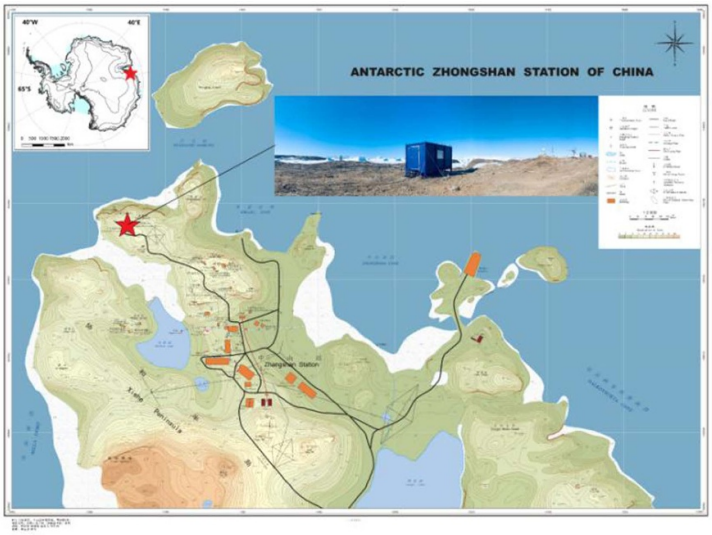

Figure 1. The location of the atmospheric chemical monitoring station and observation room in summer at ZOS.

2.3. Air mass back-trajectory calculation

The HYSPLIT back trajectory analysis is a common application to determine the origin of air masses and establish source-receptor relationships (Stein *et al* 2015). It has been proven credible in previous Antarctica researches (e.g. Legrand *et al* 2009, Hara *et al* 2011). The TrajStat tools (MeteoInfoMap plugin for air mass trajectory statistic; Wang 2014) was be used to derive the model results in this study. Because O_3 usually has a half-life of several days in troposphere (Seinfeld *et al* 1998), the backward trajectory starting height was set at 100 m above the surface, and the total run time was 120 h for each trajectory. Each run was performed at time intervals of 24 h (00:00). In order to explore the major path ways of air mass arriving at the study area, the clustering analysis was carried out based on Euclidean distance. The final cluster number was 4, which determined by the point of inflexion on a curve of total spatial variance vs. number of clusters.

2.3.1. The PSCF model

The potential source contribution function (PSCF) model has often been applied to locate air masses associated with high levels of near-surface O_3 at different sites (Dimitriou and Kassomenos 2015, Sharma *et al* 2017, Yin *et al* 2017). In the summer over the Antarctic Plateau, higher PSCF values may point to sources of NO_X released from the snow that support O_3 production. (Cristofanelli *et al* 2018). The PSCF values for the grid cells in the study domain were calculated by counting the trajectory segment endpoints that terminated within each cell (Ashbaugh *et al* 1985). If the total number of end points that fall in a cell is n_{ij} and there are m_{ij} points for which the measured O_3 parameter exceeds a criterion value selected for this parameter, then the PSCF, can be determined as

$$\mathrm{PSCF}_{ij} = \frac{m_{ij}}{n_{ij}}. \quad (1)$$

The cells with high PSCF values are associated with the arrival of air parcels at the receptor site, which has near-surface O_3 concentrations higher than the criterion value (i.e. the criterion threshold is the average concentration of non-OEEs (NOEEs) and OEEs). These cells are indicative of areas with 'high potential' contributions of the constituent. However, the identical PSCF n_{ij} values can be obtained from cells with very different counts of back-trajectory points. To explain the uncertainty due to the low values of n_{ij}, the PSCF values were scaled by a weighting function W_{ij} (Polissar *et al* 1999). The weighted PSCF (WPSCF) values when the total number of endpoints in a cell was less than approximately three times the average number of end points per cell. In this case, W_{ij} was set as follows:

$$W_{ij(\mathrm{OEE})} = \begin{cases} 1.00 & n_{ij} > 80\mathrm{Nave} \\ 0.70 & 80\mathrm{Nave} > n_{ij} > 20\mathrm{Nave} \\ 0.42 & 20\mathrm{Nave} > n_{ij} > 10\mathrm{Nave} \\ 0.05 & \mathrm{Nave} > n_{ij} \end{cases}, \quad (2)$$

where Nave represents the mean n_{ij} of all grid cells. The WPSCF values were obtained by multiplying the original PSCF values by the weighting factor.

2.3.2. The CWT model

In the PSCF model, grid cells can have identical PSCF values when sample concentrations are slightly higher or much higher than the criterion value, making it difficult for the PSCF model to distinguish between strong pollution sources and weak pollution sources. In contrast, the concentration-weighted trajectory (CWT) model can well distinguish between strong and weak pollution sources. In the CWT model, each

grid cell is assigned a weighted concentration by averaging the sample concentrations with associated trajectories crossing the grid cell, as shown below:

$$\mathrm{WCWT}_{ij} = \frac{\sum_{b=1}^{M} c_b \tau_{ijb}}{\sum_{b=1}^{M} \tau_{ijb}} \times W_{ij}, \quad (3)$$

where CWT_{ij} is the average weighted concentration in the ijth cell, b is the index of the trajectory, M is the total number of trajectories, c_b is the concentration observed on arrival of trajectory b, and τ_{ijb} is the time spent in the ijth cell by trajectory l. A high value for CWT_{ij} implies that air parcels traveling over the ijth cell would be, on average, associated with high concentrations at the receptor. Besides, the using of W_{ij} in weighted concentration weighted trajectory (WCWT) same as that in WPSCF.

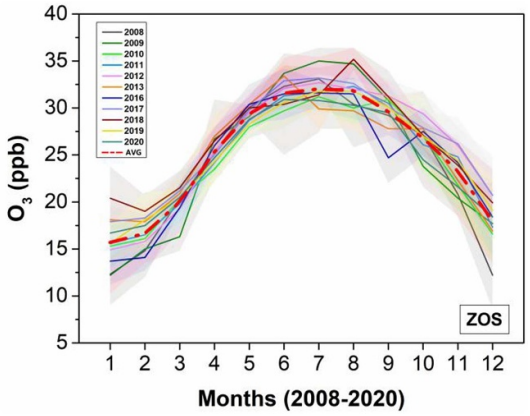

Figure 2. O_3 seasonal variations at ZOS (2008–2020). For each month, the mean value is reported with the standard deviation.

3. Results and discussion

3.1. Near-surface O_3 variability

Figure 2 shows the time series of the monthly mean O_3 concentrations at ZOS from January 2008 to December 2020. O_3 was high in winter and low in summer. The lowest O_3 concentrations (12.2–19.9 ppb) were observed in January (2009, 2010, 2011, 2012, 2016, 2017, 2019, and 2020) and December (2008, 2013, and 2018). The highest O_3 concentrations (30.9–35.2 ppb) were observed in June (2013 and 2020), July (2008, 2009, 2010, 2011, 2012, 2016, and 2017), and August (2018 and 2019), which reflect the net O_3 accumulation effect during the Antarctic polar night. As the solar altitude rises and UV irradiation increases during early spring, near-surface O_3 starts to photolyze. Moreover, the NO_X, OH^- ion (hydroxide), and HO_2 concentrations remain extremely low due to the low solar radiation, and photolysis of O_3 still dominates, leading to a considerable decrease in O_3 concentration (Monks 2000).

During the warm season (September–January), the O_3 concentration at ZOS exhibited large monthly fluctuations. This phenomenon has observed at many other coastal stations, such as the Syowa, Neumayer, Halley, and Arrival Heights stations (Ghude *et al* 2006, Helmig *et al* 2008, Wang *et al* 2011, Bian *et al* 2018). Surprisingly, abnormally high O_3 concentrations also occurred in September and October, sometimes exceeding the O_3 concentrations during the Antarctic polar night (as shown in figure 4). This phenomenon has been observed at other Antarctic inland stations, such as the SOP and Dome C (DMC) (Helmig *et al* 2008, Oltmans *et al* 2008).

To analyze the diurnal variability characteristics of O_3 at ZOS, the ΔO_3 (hourly growth rate of O_3) and diurnal variability of O_3 were calculated (figure 3(b)). The O_3 concentration at ZOS showed a clear diurnal cycle, with a maximum value at approximately 23:00 coordinated universal time (UTC) (4:00 local time (LT)) and a minimum value at approximately 9:00 UTC (14:00 LT). At ZOS, the monthly ΔO_3 varied little, ranging from −0.8 to 0.8 ppb h^{-1}, much smaller than the mean monthly ΔO_3 of 0.16 ppb h^{-1} at DMC (Cristofanelli *et al* 2018). During the polar night, the daily mean wind speed remained stable, ranging from 6 to 8 m s^{-1}, but the ΔO_3 varied greatly at times (especially from 14:00 to 22:00 LT). This could only be attributed to the strong vertical exchange between the free atmosphere and PBL.

Wind can promote mixing and transport between the PBL and the upper free atmosphere so that trace pollutants are continuously diffused in the horizontal and vertical directions. The diurnal variability of the wind speed may directly affect the reaction and transfer processes of near-surface O_3 (e.g. Argentini *et al* 2000). The O_3 concentrations continuously increase in spring and fall mornings with low wind speeds mainly because low wind speeds promote the accumulation of the O_3 precursors near the surface (Haman *et al* 2014). At the DMC, strong winds contribute to the dilution of snowpack surface-emitted O_3 precursors, which reduces the source contribution to the local photochemical process of O_3 formation (Legrand *et al* 2016). However, the wind speed at ZOS showed a notable diurnal cycle (figure 3(a)), which was positively correlated with the diurnal variability of O_3 ($r^2 = 0.983$, $P < 0.01$). This diurnal variability of O_3 at ZOS increased with wind speed, making it different from the diurnal variability of O_3 observed at DMC station. This difference may be attributed to the differences in geographical location and underlying surface between these two stations. Considering the diurnal variation characteristics of wind speed, the diurnal variability of O_3 at ZOS should be related to synoptic-scale air mass transport and the environmental background. In other words, the diurnal

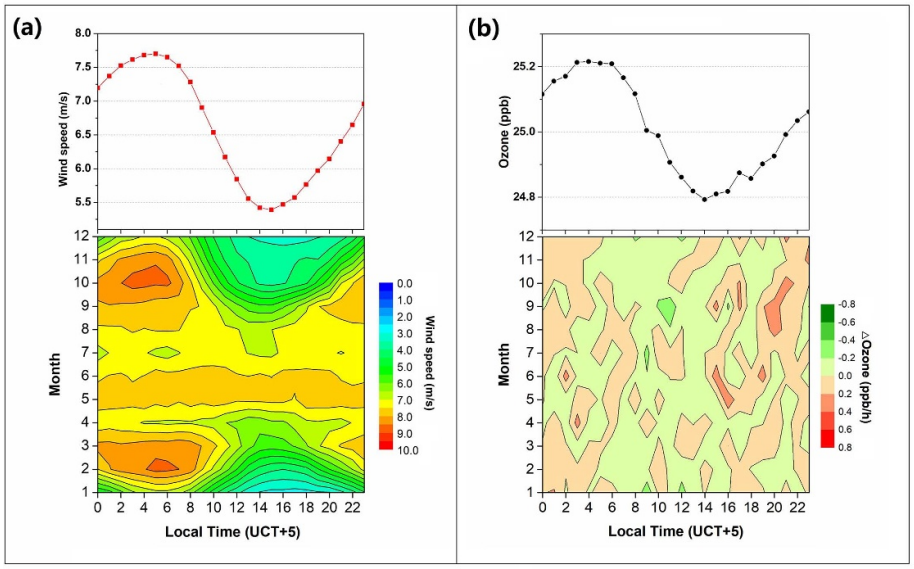

Figure 3. Monthly wind speed (a) and O_3 (b) diurnal cycles from 2008 to 2020 at ZOS. The ΔO_3 is the hourly growth rate of O_3. The point-line in the figure represents the average diurnal cycles of wind speed and O_3 from 2008 to 2020. The hot spot map shows the average daily variation characteristics of wind speed and ΔO_3 in the different months from 2008 to 2020.

variability of O_3 at ZOS can represent the background characteristics of a large area.

3.2. Identification of OEEs

Similar with the procedure in Cristofanelli *et al* (2018), the OEE day was selected based on a two-step method. First, the annual cycle of O_3 mean daily values was fitted with a sinusoidal curve. This represents an 'undisturbed' O_3 annual cycle, not affected by OEEs. In the second step, the probability density function (PDF) of the deviations from the sinusoidal fit was calculated, then a Gaussian fit was applied to the obtained PDF. It is proved that the deviations from the Gaussian distribution (calculated by using the Origin® 9 statistical tool) can be used to identify observations affected by non-background variability (e.g. Giostra *et al* 2011). In order to obtain a threshold value for selecting non-background O_3 daily values possibly affected by 'anomalous' O_3 enhancements, we computed the further Gaussian fitting of PDF points falling above 1σ (standard deviation) of the Gaussian PDF. The intersection of the two fitting curves is taken as our screening threshold (table 1).

The OEE and NOEE days at ZOS were selected (figure 4). A total of 178 d over the 11 years period were affected by OEEs: 41 d in January (23.0%), 40 d in November (22.5%), 39 d in December (21.9%), 26 d in October (14.6%),and 11 d in September (6.2%). The frequency of OEE was less than 4% during other months (figure 5). Most of the OEEs at ZOS occurred in the warm season (September–January) and its intensity was much stronger than in the cold season. And we only found three OEEs during the polar night of 2018 (2%). Besides, we did not find obvious interannual variation characteristics of OEEs during 2008–2020.

Indeed, as suggested by Chevalier *et al* (2007), the comparison between hourly and daily O_3's standard deviations were allowed to discriminate the relative contribution to the overall O_3 variability due to the diurnal variation process (PBL photochemistry and other processes) and the synoptic-scale variation process, i.e. weather change, synoptic-scale air mass transport, etc. The standard deviations based on hourly O_3 data during OEEs was minimal in January (2.9 ppb) and maximum in December (4.8 ppb). This indicated that the diurnal-scale process (i.e. PBL photochemistry and dynamics) played a role in enhancing O_3 variability during summer. However, even in December, the ratio between daily and hourly standard deviations suggested that 88.2% of O_3 variability at ZOS was associated with longer temporal scale processes.

Indeed, as suggested by Chevalier *et al* (2007), comparison of the hourly and daily O_3 standard deviations allows us to distinguish between the relative contributions of the diurnal variation processes (photochemical and other processes in the PBL) and the synoptic-scale variation processes (e.g. weather change, synoptic-scale air mass transport, etc) to the overall O_3 variability. Through calculation, we found that the annual mean contribution rate of the synoptic-scale variation processes at ZOS was 74%. In particular, the mean contribution rate of the synoptic-scale variation processes in the warm season (September–January) reached 81%. This indicates that the OEEs at ZOS are little affected by the diurnal variation processes and are mainly affected by the synoptic-scale variation processes.

Table 1. The screening threshold values for 2008–2020 at ZOS.

Year	2008	2009	2010	2011	2012	2013	2016	2017	2018	2019	2020
Threshold (ppb)	3.6	3.9	2.7	3.8	3.6	4.3	5.0	3.4	3.3	2.6	3.9

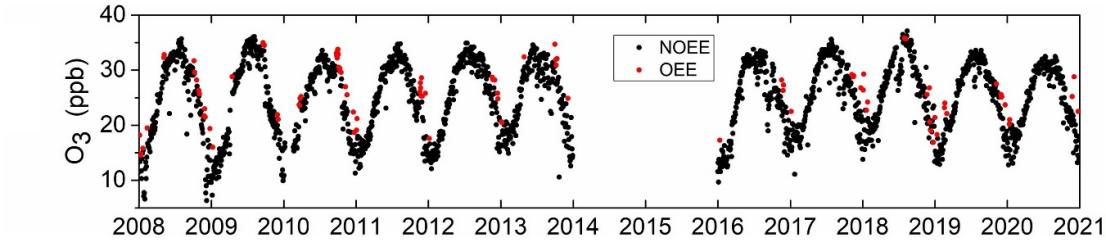

Figure 4. Daily average O_3 values during 2008–2020 at ZOS. Red and black dots represent OEE days and NOEE days, respectively.

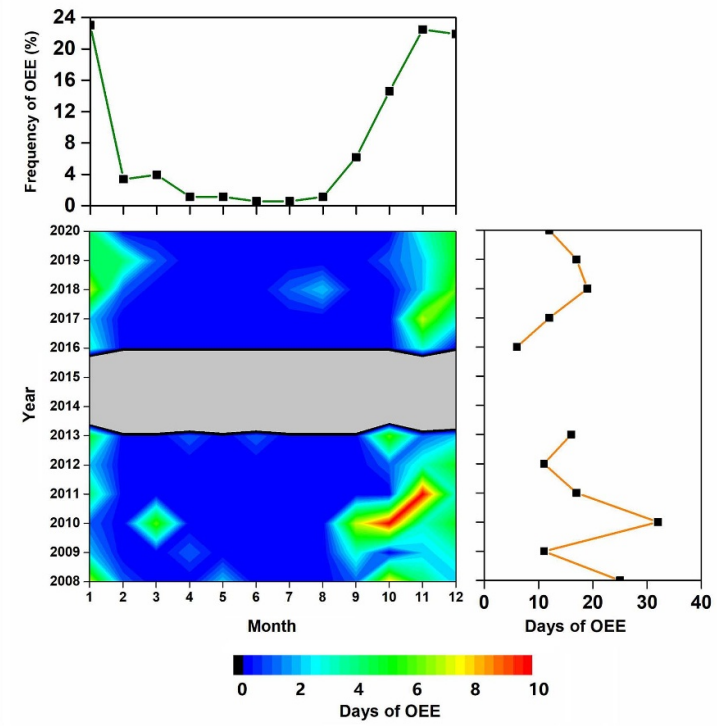

Figure 5. The OEE occurrence probability from 2008 to 2018 at ZOS.

3.3. Possible influence of the in-situ production

In Antarctica, a decrease in TCO can enhance the incident UV radiation, leading to stronger photolysis of nitrates in snowpacks and thus the release of more NO_X. This could affect *in situ* photochemical production of O_3 in the long term (e.g. Jones and Wolff 2003). Figure 6 shows the monthly mean variability of OEE frequency, TCO, and solar shortwave irradiance at ZOS. The correlation coefficient (r) between the OEE frequency and solar shortwave irradiance reached 0.91 ($P < 0.05$). This indicates that as the solar shortwave irradiance increases during early summer, the photolysis of nitrates becomes stronger, thus increasing NO_X emission (Warneck and Wurzinger 1989, Honrath *et al* 2000). The corresponding chemical reaction process is as follows: $NO_3^- + hv \rightarrow NO_2 + O^-$, $O^- + H \rightarrow OH^-$. Then, NO_2 will produce O_3 through further photochemical reactions, resulting in favorable conditions for OEEs.

As shown in figure 6, the correlation coefficient between the OEE frequency and TCO and the correlation coefficient between the OEE frequency and solar shortwave irradiance reached −0.93 and 0.99 ($P < 0.05$), respectively, during the period from July to October, providing strong evidence for the important role of stratospheric O_3 in modulating the near-surface atmospheric photochemical reaction processes by controlling UV radiation. The occurrence of

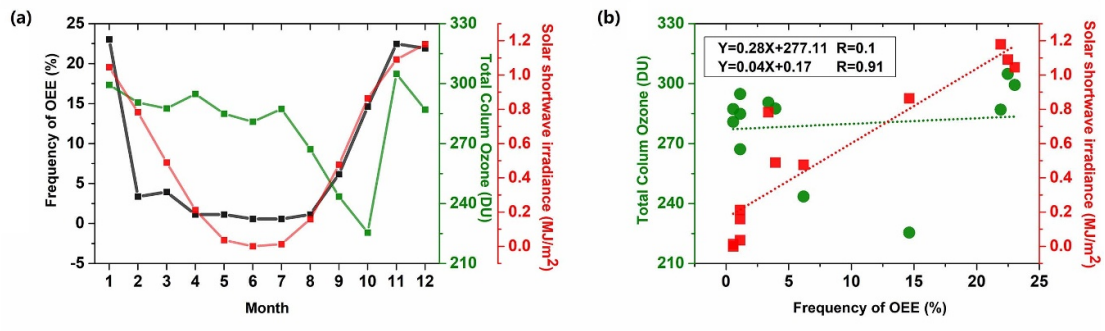

Figure 6. (a) Monthly averages of OEE frequency, TCO and solar shortwave irradiance at ZOS from 2008 to 2018; (b) linear correlation between TCO and solar shortwave irradiance with the frequency of OEE.

an O_3 hole has gradually increased the incident UV radiation (the effect of the O_3 hole on solar shortwave irradiance can be determined by calculating the difference in the slope between the solar shortwave irradiance–time curve for the period from February to May (−0.25) and that for the period from July to October (0.29)), which is also beneficial to the formation of OEEs (Jones *et al* 2000, Jones and Wolff 2003).

3.4. Role of synoptic-scale air mass transport

To better study the effect of synoptic-scale processes in triggering OEEs, we calculated the total time that air masses spent over the plateau and coastal land areas (i.e. the area within the boundaries of 90°–66.5° S and 40°–160° E) before arrival at ZOS. The time spent by air masses over all land trajectories of OEEs was approximately 3.73% of the time spent by air masses over all trajectories and was approximately 78% of the time spent by air masses over all OEE trajectories (figure 7(a)). Clearly, the total time spent by air masses over the plateau and coastal land areas significantly impacted the OEEs at ZOS (figure 7(b)). The correlation between the two reached $r = 0.82$ and passed the 99% confidence level. The finding is in agreement with Legrand *et al* (2016) and Cristofanelli *et al* (2018). Just like the conclusion drawn in section 3.2, synoptic-scale air mass transport plays a pivotal role in triggering OEEs at ZOS.

By clustering of OEE trajectories, we found that all air mass trajectories during OEEs originated from the coastal land areas of East Antarctica (the red, blue, yellow, and green lines in figure 8(a)). The O_3 concentrations of the four clusters were similar, all of them being between 20 and 31 ppb, with mean values from 25 to 27 ppb (figure 8(d)). In all months, the coastal cluster dominated during OEEs at ZOS (figure 8(c)). Furthermore, the pressures associated with the four clusters were higher than 550 hPa (figure 8(b)). These results indicate that most air masses were transported to ZOS through the troposphere over the Queen Mary Land, Wilkes Land, and Princess Elizabeth Land.

The PSCF and CWT models were applied to find the potential pollution sources of O_3 during OEEs.

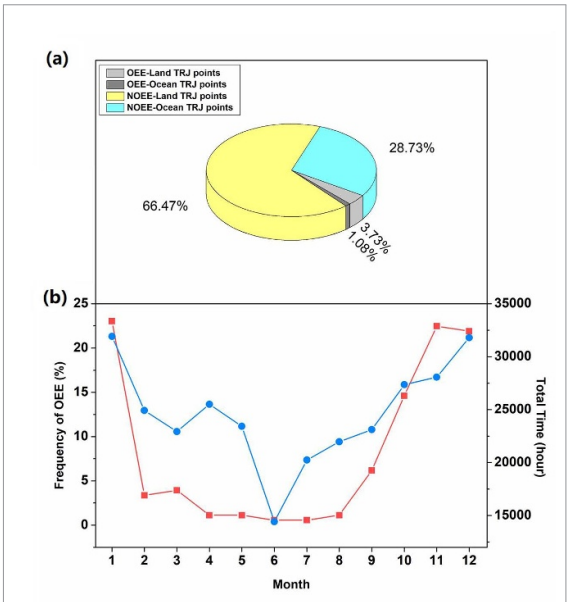

Figure 7. (a) The proportion of the different types of trajectory (TRJ) points (i.e. OEE-land TRJ, OEE-Ocean TRJ, NOEE-land TRJ, NOEE-Ocean TRJ); (b) the monthly total time spent by air masses over the plateau and coastal areas before the arrival at ZOS (blue line) versus monthly OEEs frequency (red line).

The WPSCF values were high (>0.4) in the coastal area east of ZOS (from 76° to 150° E) (figure 9(a)). The WCWT values were greater than 20 ppb in the areas east of ZOS (figure 9(b)), which also indicated that the area east of ZOS was the O_3 source region that had the greatest impact on the O_3 at ZOS. The model results further confirmed that OEEs at ZOS were mainly caused by the transport of O_3-rich air masses from the atmosphere over the coastal land areas of the Princess Elizabeth Land, Wilkes Land, and Queen Mary Land.

3.5. Role of STT events

We applied the Stratosphere-to-Troposphere Exchange Flux (STEFLUX) tool to assess the possible contribution of STT to near-surface O_3 variability of ZOS, and to determine the measurement periods

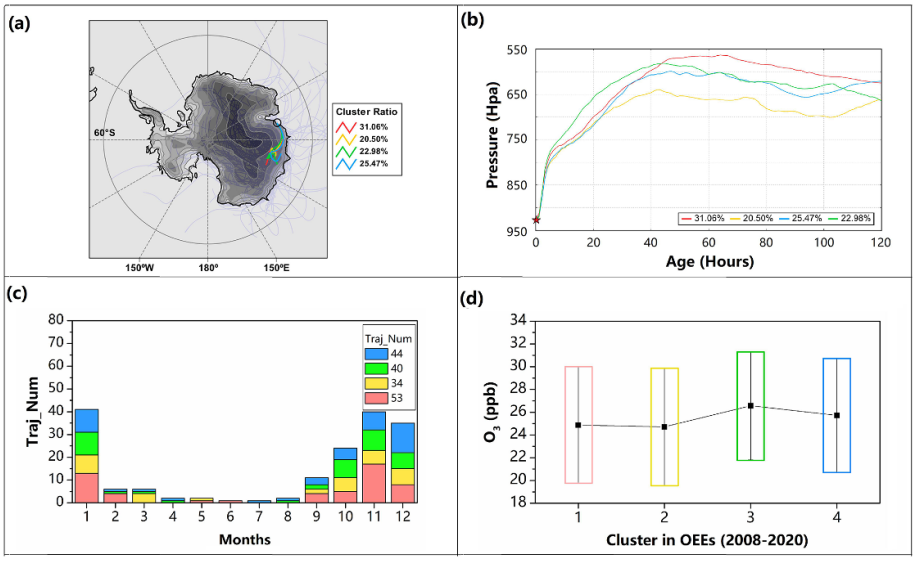

Figure 8. (a) and (b) Four clusters of HYSPLIT backward trajectories during OEEs; (c) the monthly frequency of clustering trajectories during OEEs; and (d) the range of near-surface O_3 concentrations of the four clusters. The circle and red star represents ZOS location.

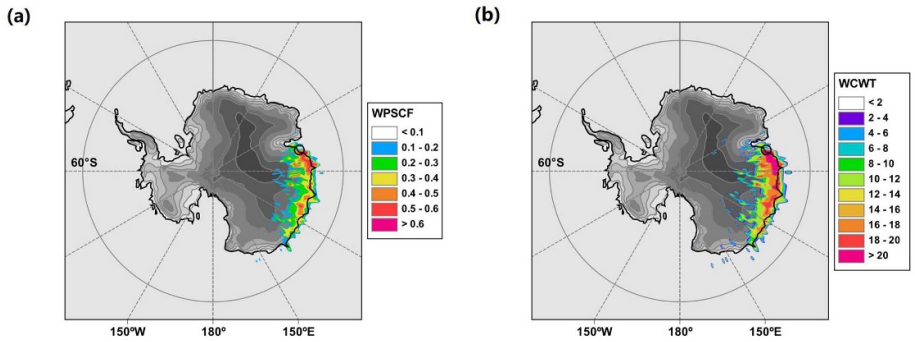

Figure 9. WPSCF (a) and WCWT (b) maps to identify the sources of O_3 derived from the PSCF and CWT models arriving ZOS at a height of 100 m above ground level.

possibly affected by STT events (i.e. stratospheric air masses transferred down to the lower troposphere). We set the top lid of the target box at 300 hPa, and the following geographical boundaries: 68°–71° S and 75°–78° E. If at least 1 stratospheric trajectory crossed the 3D target box, then a 'deep' STT event at ZOS was detected (i.e. the STEFLUX 'target box'; for further details on the methodology, see Putero *et al* 2016).

Figure 10 showed the annual (figure 10(a)) and monthly (figure 10(b)) distributions of STT events occurring at ZOS during the 2008–2018 (i.e. Since the STEFLUX tool are based on ERA-Interim data, the calculations were performed until 31 August 2018). The seasonal variation was not obvious, because of the low frequency of STT events. For example, the highest monthly frequency of STT events was only 0.9% (July). It was almost an order of magnitude lower than that of the OEEs. Therefore, it can be inferred that there was no direct link between the STT and OEE. This pattern was also reported in some previous studies (e.g. Stohl and Sodemann 2010, Cristofanelli *et al* 2018).

However, some previous studies had considered the STT process is complex on Antarctica (Roscoe 2004, Mihalikova and Kirkwood 2013). The STEFLUX is only able to consider relatively 'young' events (i.e. 4 d old). This can lead to an underestimation of the real influence of STT at ZOS. In addition, STT events can play a role by transporting nitric acid, from stratosphere to the Antarctic atmosphere, thus indirectly affecting near-surface O_3 concentration and facilitating the occurrence of OEEs (Traversi *et al* 2014, 2017). For stations on the Antarctic coast, e.g. Neumayer, stratospheric air mass intrusions in latesummer/early autumn have been proven by long-termmeasurements of $^{10}Be/^{7}Be$ in surface aerosol particles (Elsässer *et al* 2011). At ZOS, through an observational analysis of the $\Delta^{14}CO_2$, it was also confirmed that the OEE of 6 January 2011 was affected by

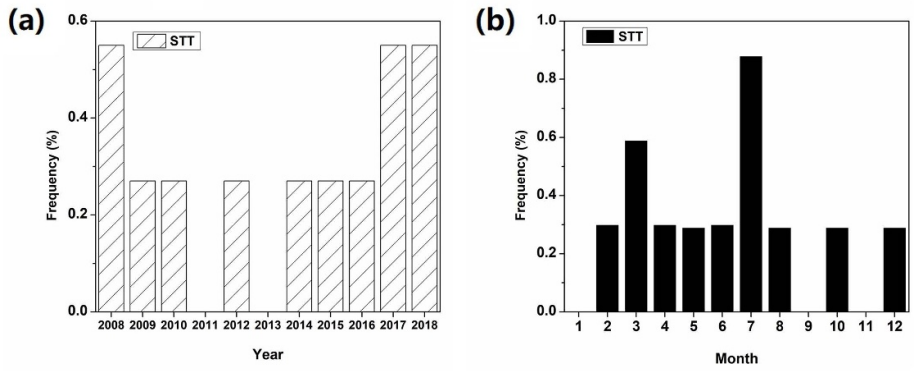

Figure 10. Annual (a) and monthly (b) distributions of 'deep' STT events at ZOS from 2008 to 2018, obtained by STEFLUX.

the STT (Zheng *et al* 2020). Therefore, it is important to carry out further studies to better assess this process.

4. Conclusion

Using observations from 2008 to 2020, the background characteristics of near-surface O_3 at ZOS in Antarctica were studied. The results suggest that synoptic-scale air mass transport controls the occurrence of OEEs, which is consistent with the findings of studies at the SOP and DMC (Neff *et al* 2008, Cristofanelli *et al* 2018). The variations in solar shortwave irradiance and TCO and their relationships with O_3 from July to October confirm that the decrease in TCO could enhance the incident UV radiation, leading to more intense photolysis of nitrates on snowpack surfaces and thus affecting the near-surface photochemical production of O_3 in the long term. In addition, this study found that STT events rarely occur at ZOS and are not directly related to the occurrence of OEEs. Unlike the OEEs at the Antarctic inland stations, the OEEs at ZOS are mainly related to the transport of air masses with high O_3 concentrations over coastal land. In summary, the synoptic-scale transport of air masses with high O_3 concentrations is the main cause of OEEs at both low-latitude coastal stations and high-latitude inland stations in Antarctica.

The mechanism by which near-surface O_3 changes at ZOS revealed in this paper is of great significance to research on atmospheric chemistry in the Antarctic region. In Antarctica, only a few observation stations have conducted long-term continuous observations of near-surface O_3. There is an urgent need for more research in this field, especially assessments of the overall regional status of near-surface O_3 based on relevant atmospheric chemistry models, which will be the focus of our future research.

Data availability statement

The data that support the findings of this study are openly available at the following URL/DOI: https://doi.org/10.11856/SNS.D.2021.001.v0. Data will be available from 19 December 2023 (Ding *et al* 2021).

Acknowledgments

This work is financially supported by the National Key Research and Development Program of China (2021YFC2802504), the National Natural Science Foundation of China (42122047, 42176240) and the Basic Fund of the Chinese Academy of Meteorological Sciences (2021Z006, 2019Y010). The observations were carried out during the Chinese National Antarctic Research Expedition at the Zhongshan Station. We are also grateful to NOAA for providing the HYSPLIT model and GFS meteorological files. Yaqiang Wang is the developer of MeteoInfo and provided generous help for the paper.

References

Argentini S, Dargaud G, Mastrantonio G, Sempreviva A M and Viola A 2000 Study of the onset and evolution of the convective boundary layer observed at the Antarctic plateau station of Dome C using a mid-latitude mixing-height model

Ashbaugh L L, Malm W C and Sadeh W Z 1985 A residence time probability analysis of sulfur concentrations at Grand Canyon National Park *Atmos. Environ.* **19** 1263–70

Bian L G, Ye L, Ding M H, Gao Z Q, Zheng X D and Schnell R C 2018 Surface ozone monitoring and background concentration at Zhongshan Station, Antarctica *Atmos. Clim. Sci.* **8** 1–14

Bonasoni P, Evangelisti F, Bonafe U, Ravegnani F, Calzolari F, Stohl A, Tositti L, Tubertini O and Colombo T 2000 Stratospheric ozone intrusion episodes recorded at Mt. Cimone during the VOTALP project: case studies *Atmos. Environ.* **34** 1355–65

Chevalier A, Gheusi F, Delmas R, Ordóñez C, Sarrat C, Zbinden R, Thouret V, Athier G and Cousin J M 2007 Influence of altitude on ozone levels and variability in the lower troposphere: a ground-based study for western Europe over the period 2001–2004 *Atmos. Chem. Phys.* **7** 4311–26

Cooper M, Martin R V, Wespes C, Coheur P, Clerbaux C and Murray L T 2014 Tropospheric nitric acid columns from the IASI satellite instrument interpreted with a chemical transport model: implications for parameterizations of nitric oxide production by lightning *J. Geophys. Res. Atmos.***119** 10068–79

Crawford J H *et al* 2001 Evidence for photochemical production of ozone at the South Pole surface *Geophys. Res. Lett.* **28** 3641–4

Cristofanelli P *et al* 2018 Analysis of multi-year near-surface ozone observations at the WMO/GAW 'Concordia' station (75°06'S, 123°20'E, 3280 m a.s.l—Antarctica) *Atmos. Environ.* **177** 54–63

Cristofanelli P, Bonasoni P, Calzolari F, Bonafè U, Lanconelli C, Lupi A, Trivellone G, Vitale V and Petkov B 2008 Analysis of near-surface ozone variations in Terra Nova Bay, Antarctica *Antarct. Sci.* **20** 415–21

Cristofanelli P, Calzolari F, Bonafè U, Lanconelli C, Lupi A, Busetto M, Vitale V, Colombo T and Bonasoni P 2011 Five-year analysis of background carbon dioxide and ozone variations during summer seasons at the Mario Zucchelli station (Antarctica) *Tellus* B **63** 831–42

David L M and Nair P R 2011 Diurnal and seasonal variability of surface ozone and NOx at a tropical coastal site: association with mesoscale and synoptic meteorological conditions *J. Geophys. Res. Atmos.* **116** D10303

Davis D *et al* 2001 Unexpected high levels of NO observed at South Pole *Geophys. Res. Lett.* **28** 3625–8

Dimitriou K and Kassomenos P 2015 Three year study of tropospheric ozone with back trajectories at a metropolitan and a medium scale urban area in Greece *Sci. Total Environ.* **502** 493–501

Ding M and Tian B 2021 *National Arctic and Antarctic Data Center* (https://doi.org/10.11856/SNS.D.2021.001.v0 Accessed 17 November 2021))

Elsässer C, Wagenbach D, Weller R, Auer M, Wallner A and Christl M 2011 Continuous 25-yr aerosol records at coastal Antarctica *Tellus B: Chem. Phys. Meteorol.* **63** 920–34

Frey M M, Roscoe H K, Kukui A, Savarino J, France J L, King M D, Legrand M and Preunkert S 2015 Atmospheric nitrogen oxides (NO and NO_2) at Dome C, East Antarctica, during the OPALE campaign *Atmos. Chem. Phys.* **15** 7859–75

Ghude S D, Jain S L, Arya B C, Kulkarni P S, Kumar A and Ahmed N 2006 Temporal and spatial varia- bility of surface ozone at Delhi and Antarctica *Int. J. Climatol.* **26** 2227–42

Giostra U, Furlani F, Arduini J, Cava D, Manning A, ODoherty S, Reimann S and Maione M 2011 The determination of a 'regional' atmospheric background mixing ratio for anthropogenic greenhouse gases: a comparison of two independent methods *Atmos. Environ.* **45** 7396–405

Gruzdev A N and Sitnov S A 1993 Tropospheric ozone annual variation and possible troposphere-stratosphere coupling in the Arctic and Antarctic as derived from ozone soundings at Resolute and Amundsen-Scott stations *Tellus* B **45** 89–98

Haman C L, Couzo E, Flynn J H, Vizuete W and Lefer B L 2014 Relationship between boundary layer heights and growth rates with ground-level ozone in Houston, Texas *J. Geophys. Res. Atmos.* **119** 6230–45

Hara K, Osada K, Nishita-Hara C and Yamanouchi T 2011 Seasonal variations and vertical features of aerosol particles in the Antarctic troposphere *Atmos. Chem. Phys.* **11** 5471–84

Helmig D, Johnson B, Oltmans S J, Neff W, Eisele F and Davis D D 2008 Elevated ozone in the boundary layer at South Pole *Atmos. Environ.* **42** 2788–803

Honrath R E, Peterson M C, Dziobak M P, Dibb J E, Arsenault M A and Green S A 2000 Release of nox from sunlight-irradiated midlatitude snow *Geophys. Res. Lett.* **27** 2237–40

Jones A E, Weller R, Wolff E W and Jacobi H W 2000 Speciation and rate of photochemical NO and NO2 production in Antarctic snow *Geophys. Res. Lett.* **27** 345–8

Jones A E and Wolff E W 2003 An analysis of the oxidation potential of the South Pole boundary layer and the influence of stratospheric ozone depletion *J. Geophys. Res. Atmos.* **108** 4565

Legrand M *et al* 2016 Inter-annual variability of surface ozone at coastal (Dumont d'Urville, 2004–2014) and inland (Concordia, 2007–2014) sites in East Antarctica *Atmos. Chem. Phys.* **16** 8053–69

Legrand M, Preunkert S, Jourdain B, Gallée H, Goutail F, Weller R and Savarino J 2009 Year-round record of surface ozone at coastal (Dumont d'Urville) and inland (Concordia) sites in East Antarctica *J. Geophys. Res. Atmos.* **114**

Lin X, Trainer M and Liu S C 1988 On the nonlinearity of the tropospheric ozone production *J. Geophys. Res. Atmos.* **93** 15879

Mihalikova M and Kirkwood S 2013 Tropopause fold occurrence rates over the Antarctic station troll (72°S, 2.5°E) *Ann. Geophys.* **31** 591–8

Monks P S 2000 A review of the observations and origins of the spring ozone maximum *Atmos. Environ.* **34** 3545–61

Monks P S, Archibald A T, Colette A, Cooper O, Coyle M, Derwent R, Fowler D, Granier C, Law K S and Mills G E 2015 Tropospheric ozone and its precursors from the urban to the global scale from air quality to short-lived climate forcer *Atmos. Chem. Phys.* **15** 8889–973

Neff W, Helmig D, Grachev A and Davis D 2008 A study of boundary layer behavior associated with high NO concentrations at the South Pole using a minisodar, tethered balloon, and sonic anemometer *Atmos. Environ.* **42** 2762–79

Oltmans S J, Johnson B J and Helmig D 2008 Episodes of high surface-ozone amounts at south pole during summer and their impact on the long-term surface-ozone variation *Atmos. Environ.* **42** 2804–16

Polissar A V, Hopke P K, Paatero P, Kaufmann Y J, Hall D K, Bodhaine B A, Dutton E G and Harris J M 1999 The aerosol at Barrow, Alaska: long-term trends and source locations *Atmos. Environ.* **33** 2441–58

Putero D, Cristofanelli P, Sprenger M, Škerlak B, Tositti L and Bonasoni P 2016 STEFLUX, a tool for investigating stratospheric intrusions: application to two WMO/GAW global stations *Atmos. Chem. Phys.* **16** 14203–17

Robinson E, Clark D, Cronn D R, Bamesberger W L and Hogan A W 1983 Stratospheric-tropospheric ozone exchange in Antarctica caused by mountain waves *J. Geophys. Res. Oceans* **88** 10708–20

Roscoe H 2004 Possible descent across the tropopause in antarctic winter *Adv. Space Res.* **33** 1048–52

Schultz M G *et al* 2015 The global atmosphere watch reactive gases measurement network *Elem. Sci. Anth.* **3**

Seinfeld J H, Pandis S N and Noone K 1998 Atmospheric chemistry and physics: from air pollution to climate change Wiley *Phys. Today* **51** 88–90

Sharma A, Mandal T K, Sharma S K, Shukla D K and Singh S 2017 Relationships of surface ozone with its precursors, particulate matter and meteorology over Delhi *J. Atmos. Chem.* **74** 451–74

Stein A F, Draxler R R, Rolph G D, Stunder B J, Cohen M D and Ngan F 2015 NOAA's HYSPLIT Atmospheric Transport and Dispersion Modeling System *Bulletin of the American Meteorological Society* **96** 2059–77

Stohl A and Sodemann H 2010 Characteristics of atmospheric transport into the Antarctic troposphere *J. Geophys. Res. Atmos.* **115** D02305

Traversi R *et al* 2014 Insights on nitrate sources a Dome C (East Antarctic Plateau) from multi-year aerosol and snow records *Tellus* B **66** 22550

Traversi R et al 2017 Multi-year record of atmospheric and snow surface nitrate in the central Antarctic plateau *Chemosphere* **172** 341–54

Wakamatsu S, Ohara T and Uno I 1996 Recent trends in precursor concentrations and oxidant distributions in the Tokyo and Osaka areas *Atmos. Environ.* **30** 0–721

Wang Y Q 2014 MeteoInfo: GIS software for meteorological data visualization and analysis *Meteorol. Appl.* **21** 360–8

Wang Y T, Bian L G, Ma F, Tang J, Zhang D Q and Zheng X D 2011 Surface ozone monitoring and background characteristic at Zhongshan station over Antarctica *Chin. Sci. Bull.* **10** 1011–9

Warneck P and Wurzinger C 1989 ChemInform abstract: product quantum yields for the 305 nm photodecomposition of NO_3 in aqueous solution *Cheminform* **20** 4

Yin X, Kang S, De Foy B, Cong Z, Luo J, Zhang L, Ma Y, Zhang G, Rupakheti D and Zhang Q 2017 Surface ozone at Nam Co in the inland Tibetan Plateau: variation, synthesis comparison and regional representativeness *Atmos. Chem. Phys.* **17** 11293–1131

Zheng X, Ding P, Han Z, Shen C, Liu K, Tang J and Bian L 2020 Measurements of atmospheric Δ^{14} CO_2 along the R/V Xuelong cruise track from Zhongshan Station (Antarctica) to Shanghai *Tellus B: Chem. Phys. Meteorol.* **72** 1–14